

RESEARCH

Open Access



Efferocytosis is restricted by axon guidance molecule EphA4 via ERK/Stat6/MERTK signaling following brain injury

Eman Soliman^{1,2}, John Leonard¹, Erwin Kristobal Gudenschwager Basso¹, Ilana Gershenson¹, Jing Ju¹, Jatia Mills¹, Caroline de Jager³, Alexandra M. Kaloss¹, Mohamed Elhassanny¹, Daniela Pereira¹, Michael Chen¹, Xia Wang¹ and Michelle H. Theus^{1,3,4,5*}

Abstract

Background Efferocytosis is a process that removes apoptotic cells and cellular debris. Clearance of these cells alleviates neuroinflammation, prevents the release of inflammatory molecules, and promotes the production of anti-inflammatory cytokines to help maintain tissue homeostasis. The underlying mechanisms by which this occurs in the brain after injury remain ill-defined.

Methods We used GFP bone marrow chimeric knockout (KO) mice to demonstrate that the axon guidance molecule EphA4 receptor tyrosine kinase is involved in suppressing MERTK in the brain to restrict efferocytosis of resident microglia and peripheral-derived monocyte/macrophages.

Results Single-cell RNAseq identified MERTK expression, the primary receptor involved in efferocytosis, on monocytes, microglia, and a subset of astrocytes in the damaged cortex following brain injury. Loss of EphA4 on infiltrating GFP-expressing immune cells improved functional outcome concomitant with enhanced efferocytosis and overall protein expression of p-MERTK, p-ERK, and p-Stat6. The percentage of GFP⁺ monocyte/macrophages and resident microglia engulfing NeuN⁺ or TUNEL⁺ cells was significantly higher in KO chimeric mice. Importantly, mRNA expression of *Mertk* and its cognate ligand *Gas6* was significantly elevated in these mice compared to the wild-type. Analysis of cell-specific expression showed that p-ERK and p-Stat6 co-localized with MERTK-expressing GFP⁺ cells in the perilesional area of the cortex following brain injury. Using an in vitro efferocytosis assay, co-culturing pHrodo-labeled apoptotic Jurkat cells and bone marrow (BM)-derived macrophages, we demonstrate that efferocytosis efficiency and mRNA expression of *Mertk* and *Gas6* was enhanced in the absence of EphA4. Selective inhibitors of ERK and Stat6 attenuated this effect, confirming that EphA4 suppresses monocyte/macrophage efferocytosis via inhibition of the ERK/Stat6 pathway.

Conclusions Our findings implicate the ERK/Stat6/MERTK axis as a novel regulator of apoptotic debris clearance in brain injury that is restricted by peripheral myeloid-derived EphA4 to prevent the resolution of inflammation.

Keywords Efferocytosis, Neuroinflammation, Traumatic brain injury, Apoptosis, Peripheral-derived macrophages, Microglia, Eph, Ephrin, MERTK

*Correspondence:

Michelle H. Theus
mtheus@vt.edu

Full list of author information is available at the end of the article



© The Author(s) 2023. **Open Access** This article is licensed under a Creative Commons Attribution 4.0 International License, which permits use, sharing, adaptation, distribution and reproduction in any medium or format, as long as you give appropriate credit to the original author(s) and the source, provide a link to the Creative Commons licence, and indicate if changes were made. The images or other third party material in this article are included in the article's Creative Commons licence, unless indicated otherwise in a credit line to the material. If material is not included in the article's Creative Commons licence and your intended use is not permitted by statutory regulation or exceeds the permitted use, you will need to obtain permission directly from the copyright holder. To view a copy of this licence, visit <http://creativecommons.org/licenses/by/4.0/>. The Creative Commons Public Domain Dedication waiver (<http://creativecommons.org/publicdomain/zero/1.0/>) applies to the data made available in this article, unless otherwise stated in a credit line to the data.

Background

Traumatic brain injury (TBI) is a major cause of morbidity and mortality worldwide [1]. Neuroinflammation is the primary driver of secondary injury after TBI, with microglia and peripheral-derived macrophages (PDMs) playing critical roles in regulating the production of pro-inflammatory mediators [2]. These two ontogenically distinct phagocytes mediate neuronal dysfunction by producing inflammatory and cytotoxic molecules while promoting neuroprotection through efferocytosis, the process of clearing apoptotic cell debris formed after tissue damage [3–5].

Efferocytosis is a complex, well-orchestrated process to remove apoptotic cell debris by phagocytes to enable the resolution of inflammation and tissue repair. However, a prolonged or excessive inflammatory response reduces efferocytosis efficiency and delays tissue recovery [5]. Recognition and engulfment of apoptotic cells are mediated by a network of interactions, including “find-me”, “eat-me”, and engulfment signals. During inflammation, apoptotic cells secrete molecules as “find-me” signals that attract phagocytes to eliminate the corpses. The cell surface expression of “eat-me” signals ensures the recognition of apoptotic cells by phagocytes. Phosphatidyl serine (PtdSer) is the most recognized “eat-me” signal expressed on the surface of apoptotic cells, which binds directly or indirectly to phagocytic receptors to initiate the engulfment. The indirect binding of PtdSer to the phagocytic receptors is mediated by engulfment signals secreted by phagocytes. PtdSer/(Gas6 or Pros1)/MERTK are well-characterized binding complexes for phagocyte efferocytosis, including macrophages and microglia. Although apoptosis is a hallmark of brain trauma and a determinant of the severity of TBI outcomes [6–8], the mechanisms regulating efferocytosis following injury remain ill-defined.

The erythropoietin-producing hepatocellular carcinoma receptors type A (EphA) are tyrosine kinase receptors which, upon activation by cell surface-bound ephrin ligands, initiate bidirectional signaling implicated in neurodevelopment [9]. Following brain trauma, EphA4 is overexpressed in the damaged cortical tissues, and global deficiency of this receptor demonstrates neuroprotection [10]. In prior work, we found that EphA4 is upregulated on both microglia and PDMs. Interestingly, conditional deletion of EphA4 in resident microglia failed to improve TBI outcomes [11]; however, peripheral EphA4 deficiency reduced neuroinflammation and showed neuroprotection [12]. The current study reveals a key mechanism by which peripheral-derived EphA4 limits the innate immune response to resolving tissue inflammation in the brain. This is the first evidence that efferocytosis occurs in a limited fashion in the brain

following a traumatic insult and that enhancing this process via targeting MERTK/EphA4 may be a novel strategy to improve outcomes.

Materials and methods

Animals

Male *Cx3cr1^{CreER/+}*, *Epha4^{fl/fl}*, *Epha4^{+/+}/ROSA^{mTmG}/Tie2-Cre*, and *Epha4^{fl/fl}/ROSA^{mTmG}/Tie2-Cre* mice were housed in an AAALAC-accredited animal facility with a 12-h light–dark cycle and food and water provided ad libitum. Animal experiments were performed following the NIH Guide for the Care and Use of Laboratory Animals and approved by the Virginia Tech Institutional Animal Care and Use Committee (IACUC; #21-044). *Epha4^{fl/fl}* recipient mice, *Epha4^{+/+}/ROSA^{mTmG}/Tie2-Cre* and *Epha4^{fl/fl}/ROSA^{mTmG}/Tie2-Cre* donor mice were used for the chimeric generation, which were bred and genotyped as previously described [10, 13, 14].

Generation of bone marrow chimeric mice

Bone marrow ablation was induced by exposing *Epha4^{fl/fl}* recipient mice (6–8 weeks) to X-ray irradiation (two doses of 550 rad at six h apart). Within 24 h of irradiation, recipient mice were intravenously injected with 3–4 million bone marrow cells (BMCs) isolated from femur and tibia of donor *Rosa26^{mtmg}/Tie2-Cre/EphA4^{+/+}* or *Rosa26^{mtmg}/Tie2-Cre/EphA4^{fl/fl}* mice as previously described [10, 12]. Recipient mice were placed on gentamycin sulfate water (1 mg/ml) for 3 days before irradiation and 2 weeks after adoptive transfer. Controlled cortical impact (CCI) injury for adoptive transfer WT (WT^{+WTBMCs}) and KO (WT^{+KOBMCs}) was performed at four weeks post-chimera generation.

Flow cytometry analysis of percent chimerism

Blood samples were drawn from chimeric WT (WT^{+WTBMCs}) and KO (WT^{+KOBMCs}) mice by cardiac puncture following euthanasia with isoflurane. Red blood cells were lysed using ACK buffer (ThermoFisher, Gaithersburg, MD), and peripheral immune cells were incubated at 1/500 in Zombie aqua (BioLegend, San Diego, CA) for 20 min, washed, then incubated with 2% FC blocker (1% FBS/2 mM EDTA in PBS) for 10 min. Cells were incubated with primary antibody (APC-CD45, BioLegend, San Diego, CA) for 20 min. BD FACSAria™ II Flow Cytometer was used to count GFP+CD45+ and GFP-CD45+ in 50 K cells/sample. Data were analyzed using FlowJo v10 (BD, Ashland, Oregon).

Controlled cortical impact injury

CCI injury was induced as previously described [10, 11]. Briefly, mice were anesthetized with subcutaneous ketamine (100 mg/kg) and xylazine (10 mg/kg) and securely

positioned in a stereotaxic frame, maintaining a body temperature of 37 °C. A midline incision was made on the sanitized and shaved scalp to expose the skull. Then, a craniectomy (4 mm diameter) was performed over the right parietal–temporal cortex (−2.5 mm A/P and 2.0 mm lateral from the bregma) using a portable drill. The injury was induced with a velocity of 5 m/s and a depth of 2 mm. The incision was sutured, and animals were monitored until recovery.

Perfusion fixation and brain serial sectioning

At 1 or 3 days post-CCI injury (dpi), mice were euthanized by subcutaneous (s.c.) injection of a combination of 150 mg/kg ketamine and 20 mg/kg xylazine and perfusion fixation was performed as previously described [11]. Five minutes before perfusion, heparin (2000 units/kg, s.c.) and sodium nitroprusside (0.75 mg/kg, s.c.) were injected. After confirming the loss of pedal reflex, cardiac perfusion of heparin (20 units/ml) in phosphate-buffered saline (PBS) was performed to clear the circulation of blood, followed by perfusion with ice-cold 4% paraformaldehyde (PFA) in PBS. Fixed brains were cryoprotected with gradient sucrose solutions, snap-frozen, embedded in OCT compound with 30% sucrose, and stored at −80 °C until sectioning. Serial coronal section (30 μm) were obtained using a cryostat (−1.1 to −2.6 mm posterior from bregma), mounted on positively charged slides (with five sections spaced 450 μm apart), and stored at −80 °C for further analysis.

Single-cell sequencing, library generation, gene ontology enrichment, and computational analyses

At 1-day post-CCI injury, CD1 mice were euthanized using isoflurane, and 4 mm × 4 mm ipsilateral (injured) cortical tissues were harvested and dissociated using a papain digest neural dissociation kit (Miltenyi Biotec). Cells were then cryopreserved in 1 ml of CryoStore® CS10 media (Stem cell technologies, Seattle, WA, USA) and sent to Medgenome for scRNAseq (Foster City, California, USA). ScRNA-seq libraries were generated using the Chromium Next GEM Single Cell 5' v2 chemistry (10×Genomics) and sequenced on a NovaSeq 6000 (Illumina). An alignment of the libraries and read counts were performed using the mouse RNA-Seq Database consisting of expression values of 358 bulk Mouse RNA-seq samples of sorted cell populations (Cell Ranger V7.0, 10X Genomics). Quality control was performed, excluding genes not expressed in at least 3 cells, and cells that do not express >200 genes (Seurat, V 4.1.0 Read10X function). Doublet Finder package, v2.0.3, was used to filter for doublets, LogNormalize was used for global-scaling normalization, and Seurat was used for clustering. Unbiased cell type recognition from scRNAseq data

was performed using Cellenics. The following markers were used for the clustering of endothelial cells (Cd31, Tie2, Cdh5, Glut1), microglia (Tmem119, Ccr2-, cx3cr1), astrocytes (GFAP, Aldh1l, sox9), and monocytes/macrophages (Ccr2, Mmp8), as well as program automated clusters by brain tissue type. We applied modularity optimization by the Louvain algorithm to iteratively group cells together and visualize the data using UMAP.

Quantitative real-time PCR

Total RNA was freshly isolated from cultured bone marrow-derived macrophages, ipsilateral (4×4 mm), or contralateral (4×4 mm) cortical tissue using TRIzol® reagent (Ambion) according to the manufacturer's instructions. RNA concentration was measured using a spectrophotometer ND-1000 (NanoDrop). DNase I treatment (for a 1000 ng RNA) was performed to degrade the genomic DNA using an amplification grade kit (Sigma Aldrich, St. Louis, MO). To synthesize cDNA, reverse transcription was performed using the iScript™ cDNA synthesis kit (Biorad, Hercules, CA). For qRT-PCR, iTaq™ Universal SYBR® Green Supermix (Biorad, Hercules, CA) and specific primers (Table 1) were used to amplify cDNA (50 ng) following the manufacturer's instructions. mRNA expression (fold change) was calculated relative to GAPDH as an internal control using the $2^{-\Delta\Delta CT}$ method.

Immunohistochemistry and confocal image analysis

Serial coronal sections were washed in PBS, subsequently blocked 2% cold water fish gelatin/0.2% Triton X-100 (Sigma, Inc.) for 2 h, and then incubated overnight with the following primary antibodies diluted in blocking solutions: Rb anti-IBA1 (Wako) antibody (1:250), Rt anti-IBA1 (Abcam) antibody (1:250), Rt anti-MERTK (ThermoFisher) antibody (1:200), Rb anti-MERTK (Abcam) antibody (1:200), Rb anti-NeuN (cell signaling) antibody (1:200), Rb anti-GFAP (cell signaling) antibody (1:200),

Table 1 Sequence of primers used in qRT-PCR

Target gene	Primer sequence 5' → 3'
<i>GAPDH</i>	F: CGT CCC GTA GAC AAA ATG GT R: TCA ATG AAG GGG TCG TTG AT
<i>Mertk</i>	F: AAG TGG ATC GCC ATC GAG AG R: GGA GTC ATT CCC CGT GTT GT
<i>Gas6</i>	F: GCT TCG GTA CAA TGG CGT T R: GAC AAG GTT ACG TTC CAG CTC
<i>Pros1</i>	F: TTG GTG GAT TCT CGC TCT GG R: GAT TGC TGA TCC GAG CAC AG
<i>Cx3cr1</i>	F: GTG AGT GAC TGG CAC TTC CTG R: AAT AAC AGG CCT CAG CAG AAT C
<i>Axl</i>	F: TCA TGT GAA GCC CAC AAT GC R: ACC TCT AGC TCC GTA GGT TGT

Rb anti-P-ERK (cell signaling) antibody (1:200), or Rb anti-P-Stat6 (cell signaling) antibody (1:150). Afterward, the sections were washed with 1×PBS and incubated with the appropriate secondary antibodies (Invitrogen) diluted (1:250) in the blocking solution for 1 h: AlexaFluor donkey anti-rabbit-594, AlexaFluor donkey anti-rat-647, AlexaFluor donkey anti-rat-594, or AlexaFluor donkey anti-rabbit-647. Following another round of washing with 1×PBS, the sections were mounted using a media containing DAPI counterstain (SouthernBiotech). Confocal images were acquired using a Zeiss 880 confocal microscope (Carl Zeiss, Oberkochen, Germany).

Stereological cell counts

Cell quantification was assessed by a blinded investigator using the optical fractionator probe function of StereoInvestigator (MicroBrightField, Williston, VT, USA) on an upright Olympus BX51TRF motorized microscope (Olympus America, Center Valley, PA, USA) with a grid size set at 450×450 mm and 150×150 mm counting frame for cortex as previously described [15, 16].

TUNEL staining, imaging and counting

TUNEL staining of serial coronal sections of perfused fixed brains was performed using the Click-iT Plus TUNEL Assay 647 (Thermo Fisher Scientific) according to the manufacturer's instructions. Serial coronal section (300 μm) were permeabilized with 0.2% Triton X-100 in phosphate-buffered saline (PBS) and incubated with the TUNEL reaction mixture containing terminal deoxynucleotidyl transferase enzyme, followed by AlexaFluor 647-conjugated nucleotides. Following the TUNEL reaction, the sections were blocked in 2% cold water fish gelatin (Sigma, Inc.) in 0.2% triton for 1 h, then incubated with Rb anti-IBA1 (Wako) or Rb anti-NeuN (cell signaling) antibody (1:200 in blocking solution) overnight. Slides were then washed with 1×PBS, treated with AlexaFluor donkey anti-rabbit-555 (1:250 in block) for 1 h, further washed with 1×PBS, and then mounted in media with DAPI counterstain (SouthernBiotech). Z-stack images were acquired using a Zeiss 880 confocal microscope (Carl-Zeiss, Oberkochen, Germany).

Western blot analysis

At 3 days post-CCI injury, mice were euthanized using isoflurane, and 4 mm x 4 mm ipsilateral (injured) or contralateral cortical tissues were harvested and freshly homogenized in RIPA lysis buffer (Pierce, ThermoFisher) containing protease/phosphatase inhibitor cocktail mix (Halt, ThermoFisher). Tissue lysate was centrifuged at 12,000 rpm for 20 min, and protein concentration was determined using BCA reagents (Thermo Fisher Scientific, Inc., Rockford, IL). Equal protein concentrations of

each sample were loaded onto SDS-PAGE gels and transferred to PVDF (BioRad, Hercules, CA) using transfer buffer (containing 190 mM glycine, 25 mM Tris, 0.5% SDS, and 20% methanol). Membranes were blocked at room temperature using Intercept® (TBS) blocking buffer (LI-COR Biosciences) for 2 h and then incubated overnight with the following primary antibodies (1:1000 in blocking solution): Rb anti-Phosphorylated MERTK (PhosphoSolutions, Aurora, CO), Rb anti-MERTK (Abcam), Rb anti-Phosphorylated ERK 1/2 (Cell signaling), Ms anti-ERK 1/2 (Cell signaling), Rb anti-Phosphorylated Stat6 (Cell signaling), Rb anti-Stat6 (Cell signaling), and Ms anti-actin (Cell signaling). Membranes were washed with TBST and then incubated with LICOR IRDye anti-rabbit and/or anti-mouse IgG (LI-COR Biosciences) for one hour. Protein bands were imaged with the LI-COR Odyssey system and quantified using Fiji Image-J software.

In vitro efferocytosis assay

Bone marrow-derived macrophages (BMDMS) culturing and treatment

GFP + bone marrow-derived cells (BMCs) were isolated from the femurs of EphA4-WT (Rosa26mtmg /Tie2-Cre/EphA4+/+) or EphA4-KO (Rosa26 mtmg/Tie2-Cre/EphA4f/f) mice and cultured (1×10⁶ cells/ml) in complete RPMI medium with fetal bovine serum (10%), L-glutamine (2 mM), penicillin/streptomycin (1%), and M-CSF (10 ng/ml) as previously described [10]. On day 5, bone marrow-derived macrophages (BMDMS) were supplemented with fresh RPMI media or pre-treated with 1 μg/ml of Escherichia coli O111:B4 LPS (Sigma Aldrich, St. Louis, MO) for 4 h, 0.5 μg/ml of mouse recombinant HMGB1 (ThermoFisher Scientific) for 4 h, 5 μg/ml of EphA4-Fc or Fc-control clustered using 1.7 μg/ml α-Fc (Sino Biological, Wayne, PA) for 1 h, 25 μM of ERK inhibitor (FR18020R, Cayman chemicals) for 4 h, 5 μM of MERTK.

inhibitor (UNC2025, Cayman Chemicals) for 4 h, or 250 nM of Stat6 inhibitor (AS1517499, Cayman Chemicals) for 4 h. Jurkat cells were cultured in complete RPMI medium, counted daily, and cell density was maintained between 2×10⁵ and 1×10⁶ cells/ml until a sufficient number of cells was obtained as required for experiments. On the day of the efferocytosis experiment, Jurkat cells 1×10⁶ cells/ml were treated with 1 μM of Staurosporine (STS, Cayman chemical) for 3 h. Apoptosis was confirmed using AlexaFluor 488 Annexin/dead cells apoptosis kit (Invitrogen) containing Annexin V (AnnV) and propidium iodide (PI) per manufacturer's instructions. ImageStream Flow cytometry was used to measure early apoptotic (AnnV+/PI-) and late apoptotic/necrotic (AnnV+/PI+) cells. More than 90% of apoptotic

(both early and late) cells were required for the engulfment assay. After STS treatment, apoptotic Jurkat cells were collected, washed with HBSS, and then stained with 0.5 μM pHrodo™ Red succinimidyl (NHS) ester (ThermoFisher). Stained live and apoptotic Jurkat cells were washed, resuspended in complete RPMI media, and added to the previously cultured BMDMS in a 10:1 ratio. Cells were incubated for 1 h, and then the non-engulfed Jurkat cells were washed off with ice-cold PBS. Adherent GFP+BMDMS engulfing pHrodo+ apoptotic Jurkat cells were fixed with ice-cold 4% PFA and counterstained with DAPI. The total number of BMDMS and BMDMS engulfing apoptotic Jurkats were counted, and the efferocytosis efficiency (BMDMS engulfing apoptotic Jurkat cells/total number of BMDMS×100) was calculated as previously described [17].

Cerebral blood flow analysis

A laser speckle contrast imaging system (RFLSI III Laser Speckle Imaging System, RWD Life Science, Dover, DE, USA) was used to scan cerebral blood flow over the right parietal cortex after performing a craniectomy (4 mm diameter). Cerebral blood flow was recorded in the region of interest (ROI, 2.5 mm diameter) for 30 s, and 4 readings for each recording were taken before injury (baseline), at 10 min, and 3 dpi. The average of the 4 readings and the percentage from the baseline were calculated for each mouse. Laser speckle contrast (LSC) and bright field images were captured at every recording.

Blood–brain barrier permeability (IgG deposition)

Serial coronal sections of perfused fixed brains were blocked in 2% cold water fish gelatin (Sigma, Inc.) in 0.2% triton for 1 h, incubated with AlexaFluor donkey anti-mouse-594 (1:250 in block) for 1 h, washed in 1×PBS, and then mounted in media with DAPI counterstain (SouthernBiotech). The volume of IgG deposition (mm³) was measured using the Cavalieri Estimator from StereoInvestigator software.

Statistical analysis

Data are presented as mean±standard error of the mean (SEM), graphed, and analyzed using the GraphPad Prism program, version 9 (GraphPad Software, Inc., San Diego, CA). Shapiro–Wilk test of normal distribution was conducted for all data, and the results confirmed that all data sets follow a normal distribution of variance. The intergroup variations were analyzed using Student's unpaired two-tailed t-test (to compare between two experimental groups), one-way analysis of variance (ANOVA) followed by Bonferroni's multiple comparisons test (to compare multiple groups with one independent variable), or two-way ANOVA followed by Šidák's

multiple comparisons test (to compare multiple groups with two independent variables). The variations were considered significant at $P < 0.05$.

Results

Efferocytosis-related gene expression across single cells in the damaged cortex

Efferocytosis has not been fully characterized in brain injury following trauma. To identify specific cell types across the damaged cortex that express efferocytosis-related genes, we conducted scRNA-seq expression analysis on cells dissociated from the ipsilateral cortex at 1-day post-CCI injury. A total of 5,000 cells were included in our analysis. Uniform Manifold Approximation and Projection (UMAP) plot shows different clusters of microglia, astrocytes, endothelial cells, pericytes, neutrophils, and monocytes/macrophages isolated from the injured cortex based on RNA gene expression (Fig. 1A). The analysis of differential expression of efferocytosis signals in different cell clusters revealed that the expression of the efferocytosis receptor *Mertk* is present predominantly in microglia and astrocytes, as well as monocyte/macrophages, and endothelial cells. Its cognate ligands, *Gas6* and *Pros1*, predominate in microglia and endothelial cells (Fig. 1B). Feature UMAPs highlight the spatial location of these genes in the different clusters, confirming their enriched expression (Fig. 1C–F).

Upregulation of *Mertk* in the ipsilateral cortex following CCI injury

To investigate the effect of CCI injury on efferocytosis-related genes, we measured temporal mRNA expression of receptors involved in apoptotic cell recognition and engulfment in the ipsilateral cortex at 1, 3, and 7 dpi. We observed a significant increase in recognition receptors (*S1pr1* and *Cx3cr1*), engulfment receptors (*Mertk*), and bridging molecules (*Gas6* and *Pros1*) at 1, 3, and 7dpi (Fig. 2A–E). To determine if MERTK protein is upregulated in *Cx3cr1*-expressing cells following CCI injury, we used *Cx3cr1^{CreER}* mice, which express EYFP in *Cx3cr1*-positive cells. Immunohistochemical analysis using Iba1 (a marker for microglia and PDM) revealed increased MERTK expression on IBA1+/*Cx3cr1^{EYFP+}* cells located in the peri-lesion at 3 dpi compared to the contralateral cortex (Fig. 2G–O). To distinguish between microglia and PDMs, we used GFP bone marrow chimeric wild-type mice. Quantification of MERTK was measured in serial coronal sections immuno-stained for IBA1 at 1 and 3 dpi. The estimated number of MERTK+/*GFP+*/IBA1+ PDMs and MERTK+/*GFP-*/IBA+ microglia was measured in the ipsilateral cortex using non-biased stereology via an optical fractionator probe in the StereoInvestigator program. Consistent with scRNAseq data,

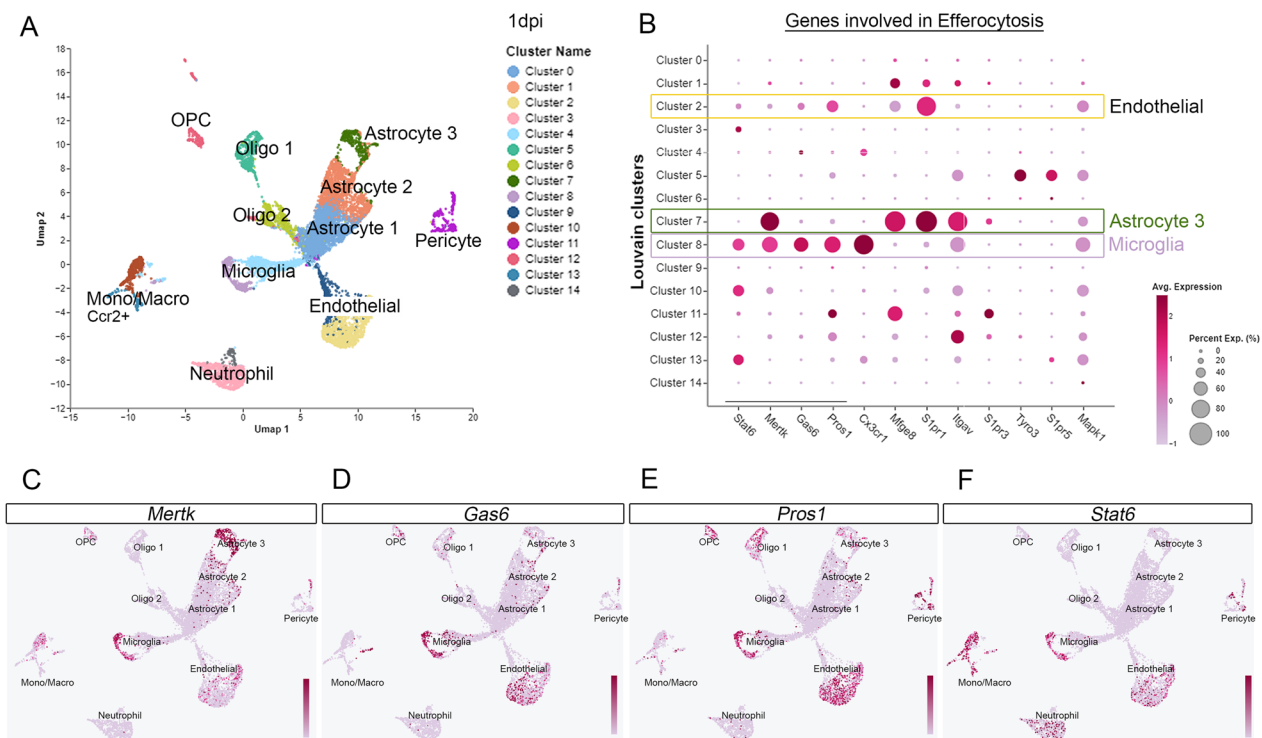


Fig. 1 ScRNA-seq analysis displays a differential expression of efferocytosis signals in the brain following CCI injury. **A** Uniform Manifold Approximation and Projection (UMAP) plot showing different cell clusters and their cell-specific annotation in the injured cortex at 1dpi. **B** Dot plot of efferocytosis genes expressed by each cluster type. **C–F** Feature maps highlighting the expression across clusters of MERTK (**C**), Gas 6 (**D**), Pros1 (**E**), and Stat6 (**F**)

(See figure on next page.)

Fig. 2 Efferocytosis-related gene changes and MERTK expression in the damaged cortex following CCI injury. **A–F** Relative mRNA expression of *Mertk* (**A**), *Gas6* (**B**), *Pros1* (**C**), *S1pr1* (**D**), *Cx3cr1* (**E**), and *Axl* (**F**) in the ipsilateral cortex of CCI-injured wild type mice at 1, 3, and 7 dpi. **G–O** Representative confocal images for MERTK expression in the wild-type *Cx3cr1^{EGFP-CreER}/+* mice at 3 dpi. **G** 2 × 2 tile confocal images for the ipsilateral cortex showing MERTK (purple), *Cx3cr1* (green), and IBA1 (red) expression. MERTK is upregulated and co-localized with *Cx3cr1* and IBA1 in the ipsilateral cortex (**H–K**). MERTK expression is low in *Cx3cr1*⁺ IBA1⁺ cells in the contralateral cortex (**L–O**). **P–Z** MERTK expression in microglia and PDM in the ipsilateral cortex of CCI-injured GFP⁺ bone marrow chimeric wild type (WT^{WTBMC}) mice. MERTK (red) is upregulated in GFP⁺ IBA1⁺ microglia at 1dpi (**P, S–V**) and 3dpi (**Q, W–Z**) and in GFP⁺ IBA1⁺ PDM at 3 dpi (**Q, W–Z**). **R** The total number of MERTK⁺ GFP⁺ IBA1⁺ microglia and MERTK⁺ GFP⁺ IBA1⁺ PDM was counted in the ipsilateral cortex at 1- and 3- dpi using the optical fractionator probe function of StereoInvestigator. *N* = 5–6 mice/group. **P* < 0.05; ***P* < 0.01; ****P* < 0.001, *****P* < 0.0001. Two-way ANOVA followed by Sidák's multiple comparisons test. Scale bar = 200 μm in **G**, 50 μm in **H–Q** and 10 μm in **S–Z**

MERTK expression was present on microglia and PDMs; however, more microglia were positive for MERTK at 1dpi. MERTK⁺ microglia count remained consistent at 3dpi, however, the estimated number of PDMs expressing MERTK was much higher. This could reflect the increased trafficking of monocytes to the brain at this time point (Fig. 2P–Z). Therefore, we show a distinct temporal change in the expression of MERTK across two distinct myeloid populations following brain injury.

Single-cell RNAseq analysis revealed an astrocyte cluster expressing *Mertk* mRNA at 1 dpi, implying a potential role in the engulfment process following CCI injury. Therefore,

we conducted immunostaining of brain sections using GFAP and MERTK to assess whether MERTK protein is upregulated in astrocytes at 3 dpi. Our findings revealed that astrocytes constituted less than 10% of MERTK-positive cells, in contrast to the 85% prevalence among PDMs and 13% in microglia (Additional file 1: Fig. S1A–K), indicating a limited role of astrocyte MERTK in the efferocytosis process.

Efferocytosis-related gene expression

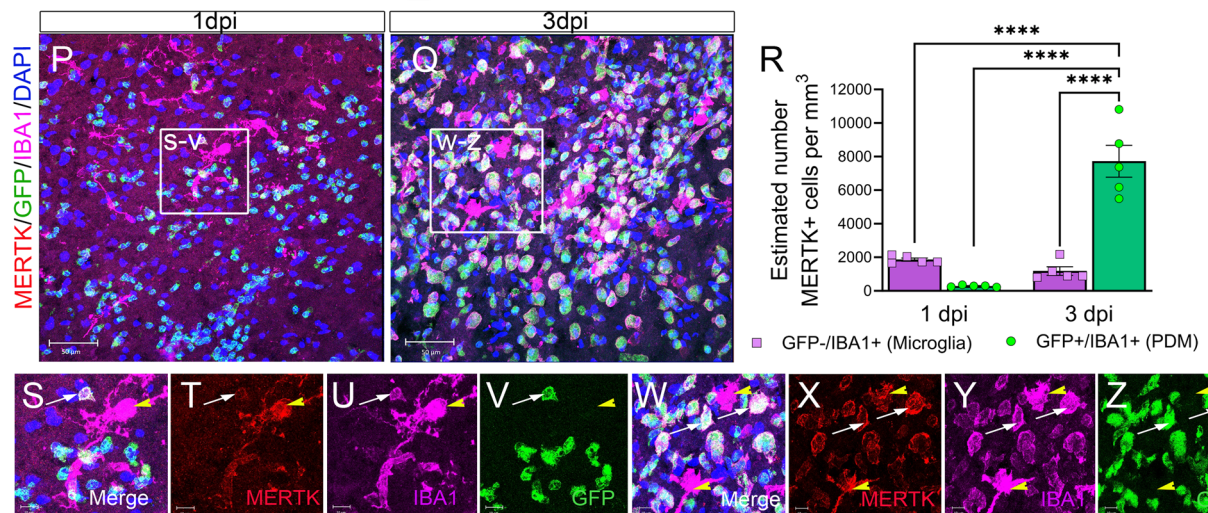
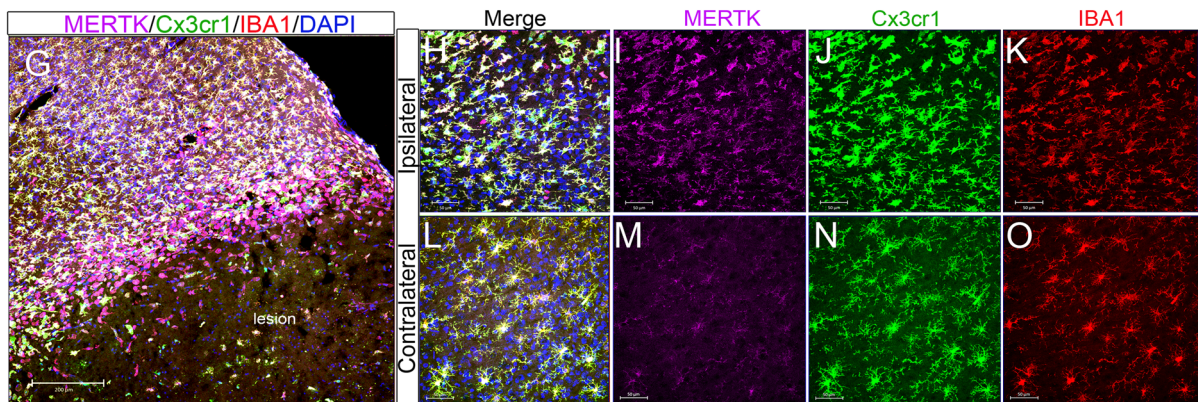
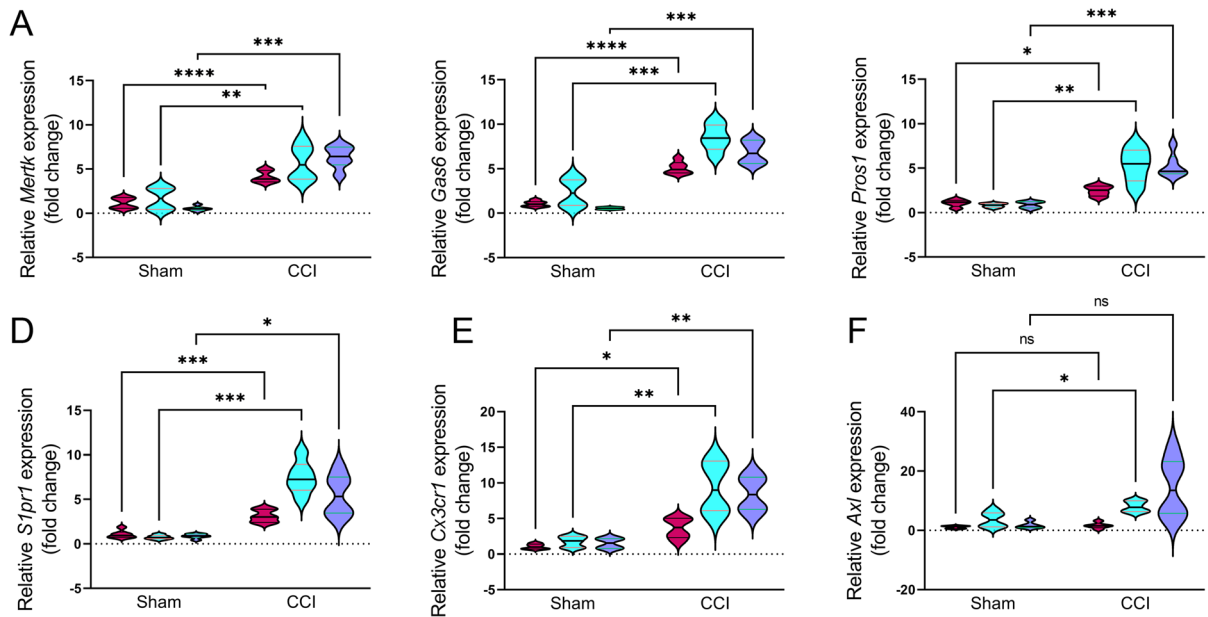


Fig. 2 (See legend on previous page.)

Initiation of efferocytosis by Cx3cr1 + microglia/macrophages following CCI injury

To determine if the change in MERTK expression in microglia and PDMs is correlated with the initiation of apoptotic neuron engulfment, coronal sections of CCI-injured *Cx3cr1^{CreER}* mice were stained with TUNEL and anti-NeuN antibody (Fig. 3). Z-stacked confocal images show *Cx3cr1^{EYFP+}* efferocytes containing DAPI+/TUNEL+, DAPI+/NeuN+, and DAPI+/TUNEL+/NeuN+ nuclei along with DAPI+/NeuN-/TUNEL- nuclei in the peri-lesion cortex at 3 dpi (Fig. 3F–O). We also observed several GFAP+ astrocytes approaching GFP+ and NeuN+ cells within the peri-lesion cortex (Additional file 2: Fig. S2A–E). However, due to the

complex morphology of astrocytes and their non-amoeboid shape, confirming the actual engulfment of other cells by astrocytes presents a challenging endeavor and requires further investigation. Therefore, our data provide the first evidence for the engulfment of dead/dying neurons by microglia and PDMs in traumatic brain-injured mice.

EphA4 deficiency in PDMs enhances the clearance of apoptotic debris in the damaged cortex following CCI injury

To evaluate the role of peripheral-derived EphA4 in this response, we used WT (*WT^{+WTBMCs}*) and EphA4 KO (*WT^{+KOBMCs}*) GFP BM chimeric KO mice. Bone marrow

Engulfment of cells in the peri-lesion cortex

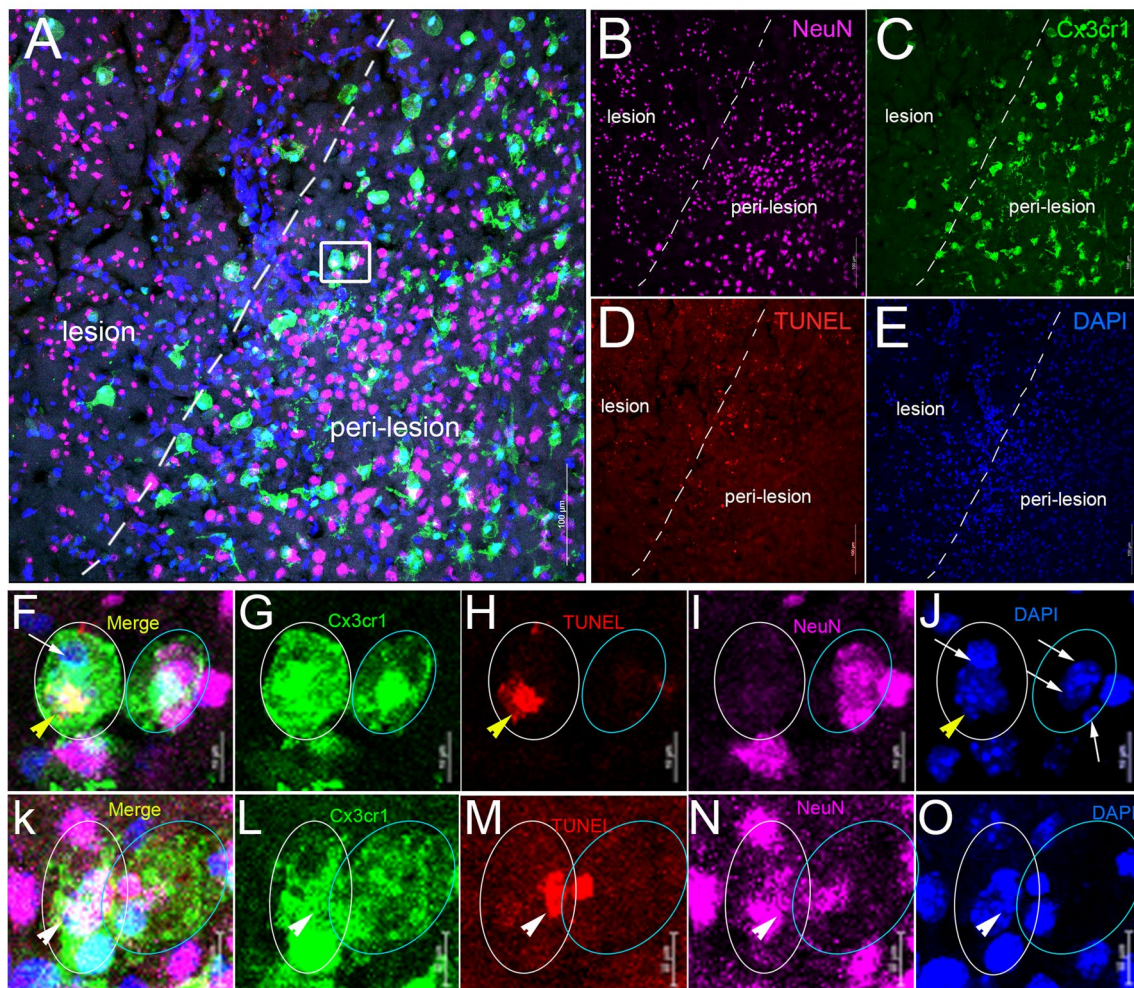


Fig. 3 Engulfment of apoptotic neurons by Cx3cr1-expressing microglia/macrophages in the injured cortex following CCI. **A–E** Representative confocal images for TUNEL (red, **D**)- and NeuN (purple, **B**)-stained coronal section of *Cx3cr1^{EYFP-CreER/+}* mice at 3 dpi. **F–O** Region of interest (ROI) showing Cx3cr1+ cells (green) containing TUNEL+ cells (yellow arrowhead), NeuN+ cells (white arrow), and TUNEL+/NeuN+ cells (white arrowhead) in the peri-lesion cortex. Scale bar = 100 μm in **A–E** and 10 μm in **F–O**

chimerism was verified by observing 94% and 96% of peripheral GFP⁺/CD45⁺ immune cells in WT⁺WTBMCs and WT⁺KOBMCs mice, respectively. A non-significant difference in GFP⁺CD45⁺ count was observed in WT⁺WTBMCs and WT⁺KOBMCs mice (Additional file 3: Fig. S3). We stained serial coronal sections of CCI-injured WT⁺WTBMCs and WT⁺KOBMCs GFP BM chimeric mice with anti-IBA1, anti-NeuN, or TUNEL and counted the percentage of PDMs (GFP⁺/IBA1⁺) and microglia (GFP⁻/IBA⁺) engulfing other cells, including peripheral immune cells (cells contain two or more DAPI⁺ nuclei including GFP cells; Fig. 4A–D), neurons (cells contain at least one NeuN⁺ cell and one DAPI⁺ nuclei; Fig. 4E–H), or TUNEL⁺ cells (cells contain at least one TUNEL⁺ and one TUNEL⁻ nuclei; Fig. 4I–K) in the core and/or perilesion of the injured cortex. We found that the percentage of PDMs and microglia containing 2⁺ nuclei is significantly higher in the lesion core (Fig. 4C) and perilesion (Fig. 4D) of WT⁺KOBMCs than in WT⁺WTBMCs. The percentage of PDMs engulfing NeuN⁺ cells in the lesion core (Fig. 4G) and the peri-lesion (Fig. 4H), as well as TUNEL⁺ cells in the lesion core (Fig. 4K), is higher in WT⁺KOBMCs than WT⁺WTBMCs. Microglia engulfing NeuN⁺ cells are significantly higher in the peri-lesion of WT⁺KOBMCs than WT⁺WTBMCs. No significant difference was observed in microglia engulfing NeuN⁺ or TUNEL⁺ cells in the lesion core. This data suggests that EphA4 deficiency in BM-derived immune cells enhances the efferocytosis capacity of PDMs and peri-lesional microglia.

Deficiency of peripheral-derived EphA4 enhances ERK/Stat6/MERTK signaling in the CCI-injured cortex

Given that myeloid MERTK-mediated efferocytosis signaling may be predominant in the brain following CCI injury and is enhanced in the absence of EphA4 (Figs. 1, 2), we sought to investigate the mRNA and protein phosphorylation status of key players in this pathway. We found that mRNA expression of *Mertk* and *Gas6* was significantly higher in the ipsilateral cortex of WT⁺KOBMCs at 3dpi when compared to WT⁺WTBMCs (Fig. 5A, B). No significant difference was observed in *Pros1* transcript (Fig. 5C). Further, Western blot analysis showed increased phosphorylation of MERTK (P-MERTK), ERK 1/2 (P-ERK), and Stat6 (P-Stat6) in the ipsilateral cortex of WT⁺KOBMCs at 3 dpi compared to WT⁺WTBMCs (Fig. 5D and Additional file 4: Fig. S4). To specifically address whether ERK and Stat6 are present on MERTK-expressing cells, coronal sections were immune-stained with anti-MERTK and anti-P-ERK (Fig. 5E and F) or

anti-MERTK and anti-P-Stat6 (Fig. 5G and H). Confocal images show colocalization of P-ERK and P-Stat6 with MERTK in the ipsilateral cortex of WT⁺KOBMCs mice and that Stat6 is increased on GFP-expressing cells in KO mice compared to WT. This indicates the co-expression of these key signaling molecules on infiltrating efferocytes.

Enhanced efferocytosis in EphA4-deficient bone marrow-derived macrophages (BMDMs) is mediated by ERK/Stat6 pathway

To confirm that EphA4 deficiency in bone marrow-derived macrophages enhances the clearance of apoptotic debris, an in vitro efferocytosis assay was performed. GFP⁺BMDMs from *Epha4*^{+/+}/*ROSA*^{mTmG}/*Tie2-Cre* (WT) or *Epha4*^{fl/fl}/*ROSA*^{mTmG}/*Tie2-Cre* (KO) mice were co-cultured with pHrodo-stained live or apoptotic Jurkat cells. Apoptosis was induced by treating Jurkat cells with staurosporine. After 3 h of treatment, 90% of Jurkat cells were in the early phase of apoptosis (Annexin V⁺ and PI⁻, Additional file 5: Fig. S5). No engulfment of live Jurkat cells was observed in EphA4 WT or EphA4 KO macrophages (Fig. 6A–H). More engulfment of apoptotic Jurkat cells was observed in untreated, LPS-treated, and HMGB1-treated EphA4 KO macrophages when compared to WT (Fig. 6I). Importantly, treating macrophages with EphA4-FC clusters (to activate the reverse ephrin signaling) did not reduce the efferocytosis efficiency of EphA4 KO macrophages, confirming that the enhanced efferocytosis in KO macrophages is mediated by the blockade of EphA4 forward signals (Fig. 6J). In addition, *Mertk* and *Gas6* expression is significantly upregulated in EphA4 KO macrophages in the absence of apoptotic Jurkat cells compared to WT macrophages. After engulfing apoptotic Jurkat cells, *Mertk* and *Gas6* expression increased in WT and KO macrophages; however, the expression is significantly higher in KO than in WT macrophages (Fig. 6K, L). *Pros1* expression increased only in EphA4 KO macrophages after apoptotic Jurkat cell engulfment (Fig. 6M). To determine if enhanced efferocytosis in EphA4 KO macrophages is mediated by MERTK, ERK, and Stat6 activation, selective inhibitors were used. MERTK inhibitor (UNC2250) reduced efferocytosis efficiency of both WT and KO macrophages; however, ERK inhibitor (FR18020R) and Stat6 inhibitor (AS1517499) selectively reduced efferocytosis efficiency of EphA4 KO macrophages (Fig. 6N). Interestingly, ERK inhibition reduced *Mertk* expression in EphA4 KO macrophages engulfing apoptotic cells, and Stat6 inhibition

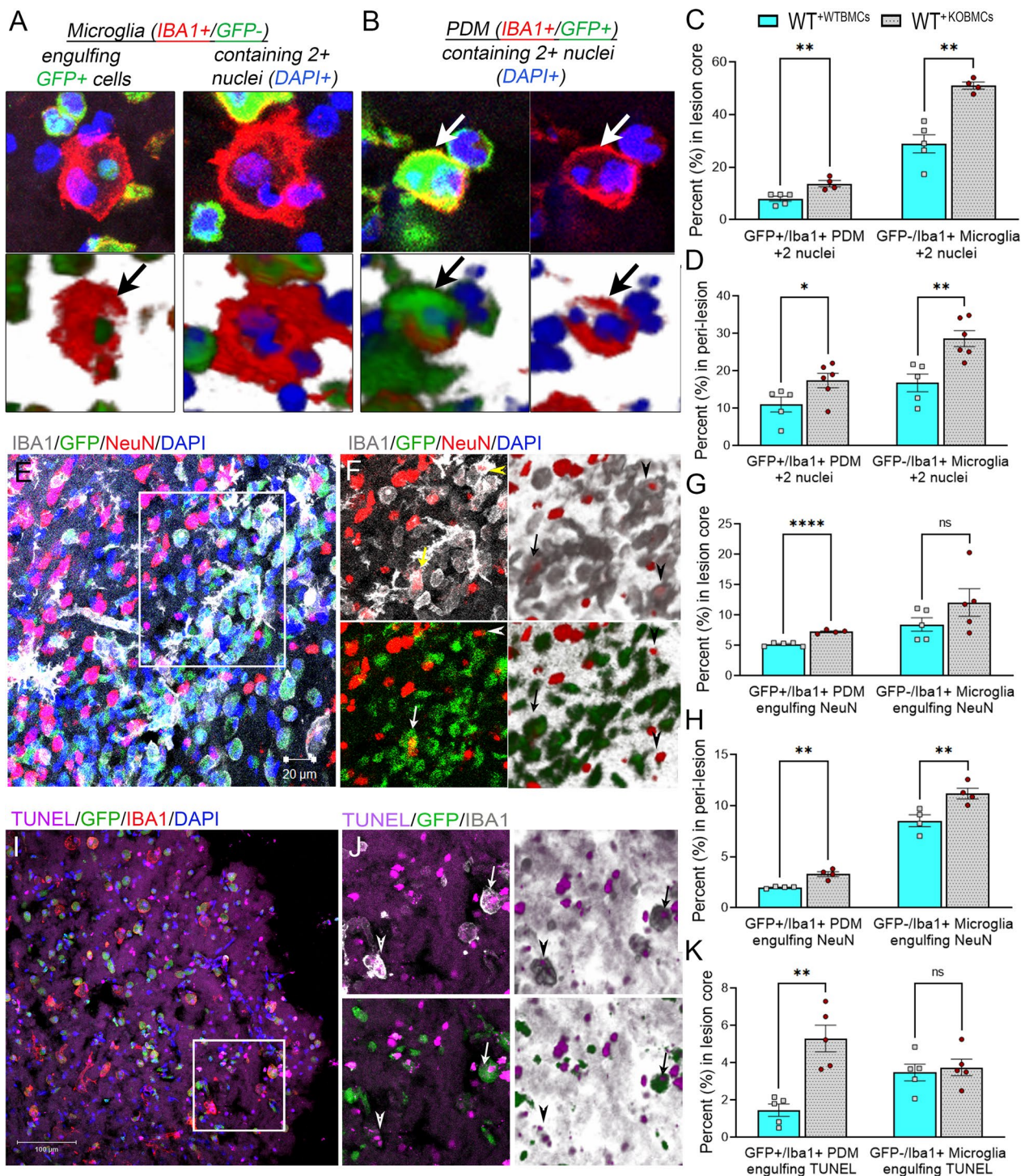


Fig. 4 Peripheral-immune EphA4 deficiency enhances efferocytosis of PDMs and microglia in the damaged cortex following CCI injury. Serial coronal sections of WT^{+WTBMCs} and WT^{+KOBMCs} mice were stained with IBA1 (red) (**A**, **B**), NeuN (red), and IBA1 (gray) (**E**, **F**), or TUNEL and IBA1 (**I**, **J**). **A**, **B** Representative images showing microglia (IBA1 +/GFP -) engulfing GFP+ cells (**A**, left) and containing 2+ nuclei (IBA1 +/GFP +) containing 2+ nuclei (**B**, right). **C**, **D** Quantification of microglia and PDM containing 2+ nuclei in the core and peri-lesion at 3dpi. **E**, **F** Microglia (arrowhead) and PDM (arrow) engulfing NeuN+ neurons. **G**, **H** Quantification of microglia and PDM engulfing NeuN+ neurons. **I**, **J** Microglia (arrowhead) and PDM (arrow) engulfing TUNEL+ nuclei. **K**, **L** Quantification of microglia and PDM containing at least one TUNEL+ nucleus and one TUNEL-DAPI+ nucleus in the core at 3dpi. $N=4-6$ mice/group. ns = non-significant; * $P < 0.05$; ** $P < 0.01$; *** $P < 0.001$; **** $P < 0.0001$. Multiple t-tests. Scale bar = 20 μm in **E** and 100 μm in **I**

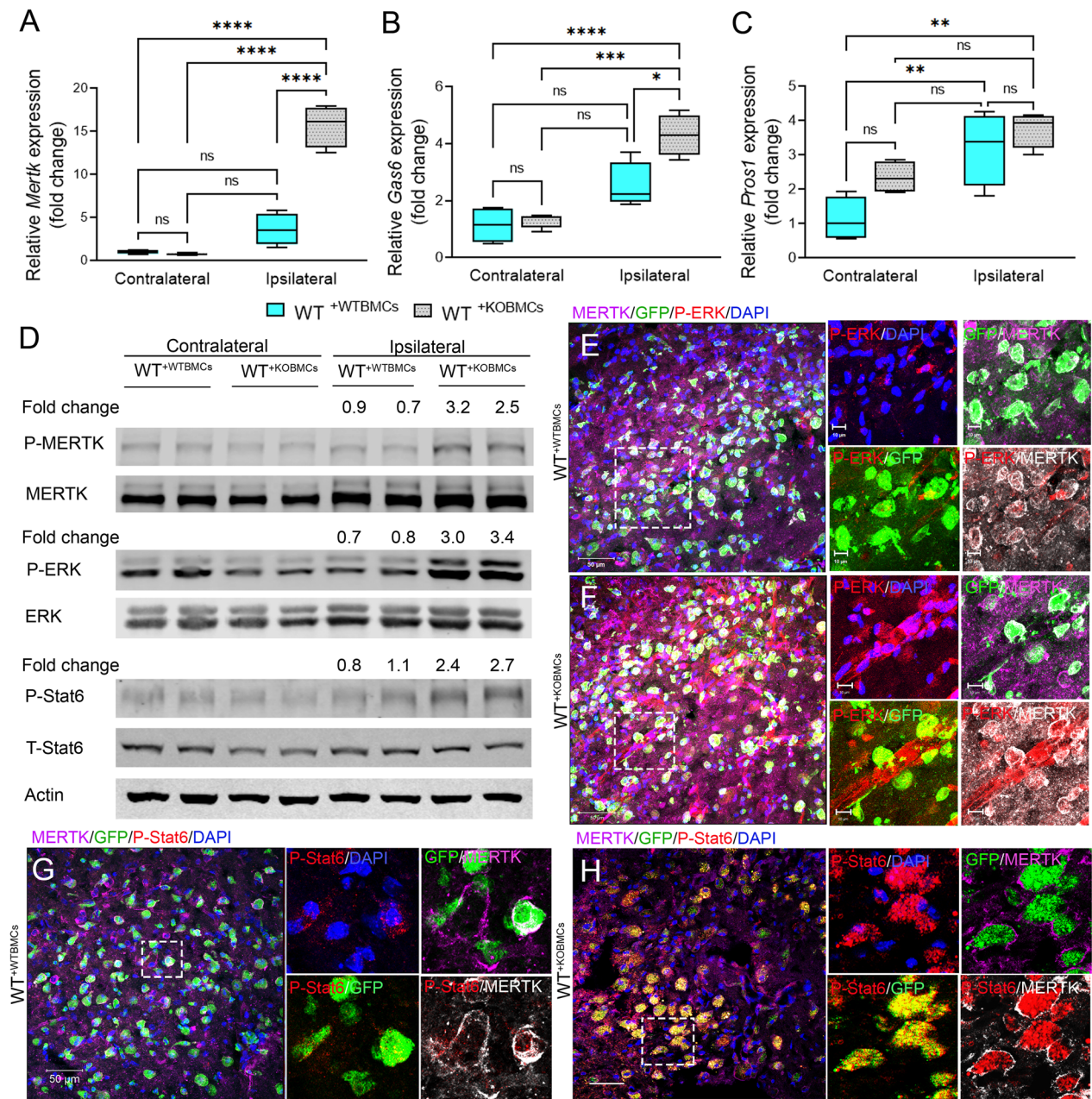


Fig. 5 Peripheral EphA4 deficiency promotes P-ERK/P-Stat6/MERTK signaling. **A–C** mRNA expression of the efferocytosis receptor (MERTK, **A**) and its ligands (*Gas6*, **B**) and (*Pros1*, **C**) in the contralateral and ipsilateral cortex of WT+^{WTBMCs} and WT+^{KOBMCs} mice at 3dpi. *N* = 5–6 mice/group. Ns = non-significant; **P* < 0.05; ***P* < 0.01; ****P* < 0.001, *****P* < 0.0001. Two-way ANOVA followed by Šidák’s multiple comparisons test. **D** Western blot analysis shows increased MERTK, ERK, and Stat6 phosphorylation in the ipsilateral cortex of chimeric WT+^{KO}BMCs mice. **E–H** Representative images showing peripheral-derived GFP+ cells expressing MERTK (purple) and P-ERK (**E, F**) and P-Stat6 (**G, H**) in WT+^{WT}BMCs and WT+^{KO}BMCs mice. Scale bar = 50 μm in **E, F, G, H** and 10 μm in insets

reduced *Mertk* and *Gas6* expression. A non-significant difference was observed in *Pros1* expression in the presence of ERK or Stat6 inhibitors (Fig. 6O). Data suggest that EphA4 forward signaling reduces macrophage

efferocytosis by inhibiting ERK and Stat6 activation, which in turn reduces the expression of efferocytosis receptor (MERTK) and its ligand (*Gas6*) and restricts the efferocytosis process (Fig. 6P).

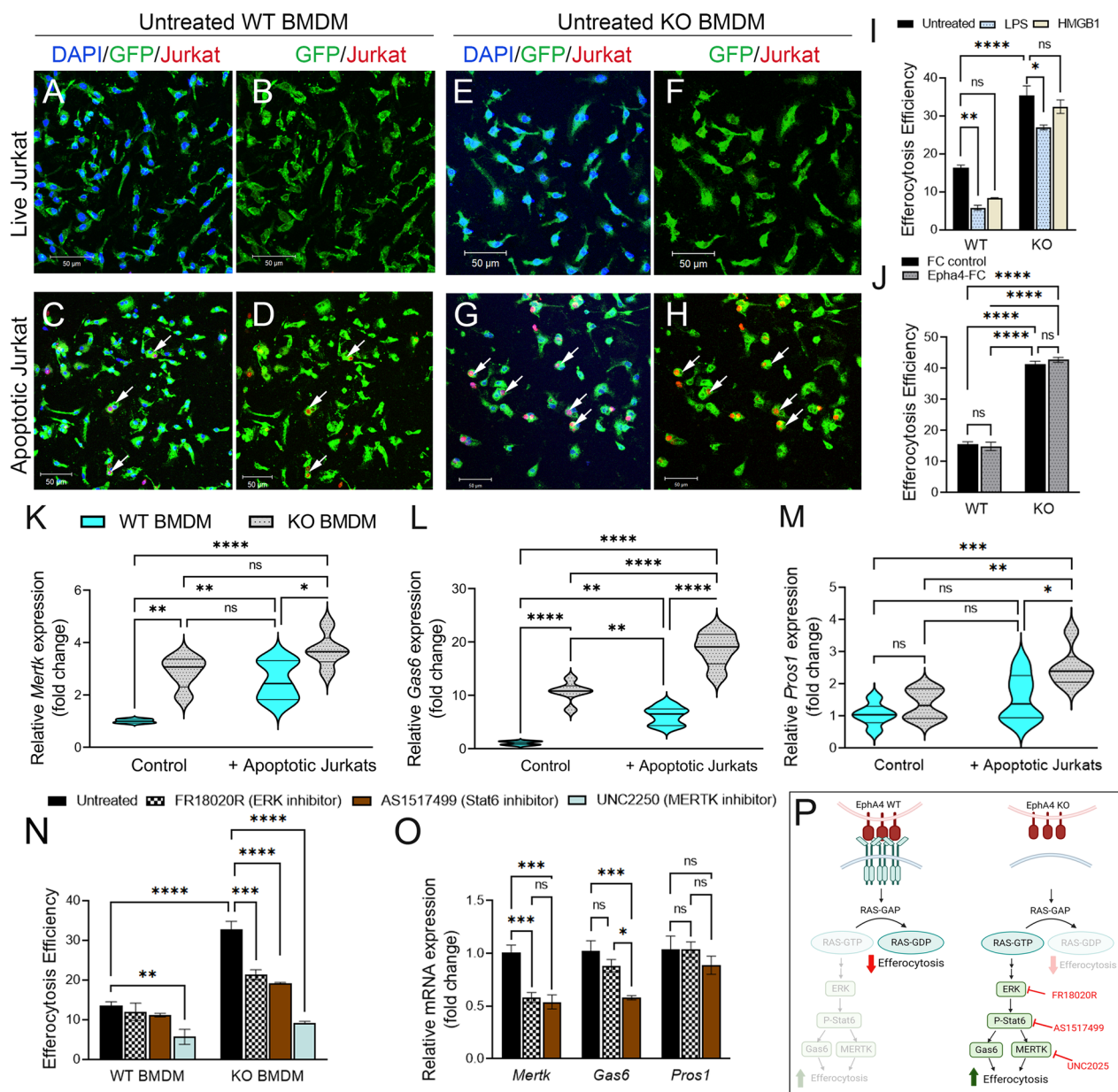


Fig. 6 EphA4-null BMDMs show enhanced efferocytosis regulated by ERK/ Stat6/MERTK. **A–H** Representative images showing the engulfment of the pHrodo-stained apoptotic (but not live) Jurkat cells (red) by GFP + untreated WT (**A–D**) and EphA4 KO (**E–H**) BMDMs. **I** Quantification of the efferocytosis efficiency of WT and EphA4 KO BMDMs after stimulation with LPS and HMGB1 for 4 h. **J** Efferocytosis of EphA4 KO BMDMs is mediated by the blockade of forward EphA4, not reverse ephrin signals. Treatment of WT and EphA4 KO BMDMs with clustered EphA4-FC to activate reverse ephrin signals did not reduce the efferocytosis of EphA4 KO BMDMs. **K–M** mRNA expression of *Mertk* (**K**), *Gas6* (**L**), and *Pros1* (**M**) with and without engulfment of apoptotic Jurkat cells. EphA4 KO BMDMs have higher expression of *Mertk* and *Gas6* than WT. **N** The use of MERTK inhibitor reduced efferocytosis of both WT and EphA4 KO BMDMs; however, Stat6 and ERK inhibitors selectively reduced efferocytosis in EphA4 KO BMDMs. **O** Stat6 inhibitor reduced *Mertk* and *Gas6* expression, and ERK inhibitor reduced *Gas6* expression in KO BMDMs engulfing apoptotic Jurkat cells. **P** Suggested pathway for the regulation of efferocytosis by EphA4. *N* = 5–6 mice/group. *Ns* = non-significant; **P* < 0.05; ***P* < 0.01; ****P* < 0.001, *****P* < 0.0001. Two-way ANOVA followed by Šidák’s multiple comparisons test (**I–N**) or one-way ANOVA followed by Tukey’s multiple comparisons test (**O**). Scale bar = 50 μm in **A–H**

Peripheral EphA4 deficiency reduced apoptotic cell counts and improved functional outcomes following CCI injury
 To determine if enhanced efferocytosis in bone marrow

chimeric EphA4 KO mice is associated with a reduction in the number of remaining uncleared apoptotic cells, the number of TUNEL + cells was counted

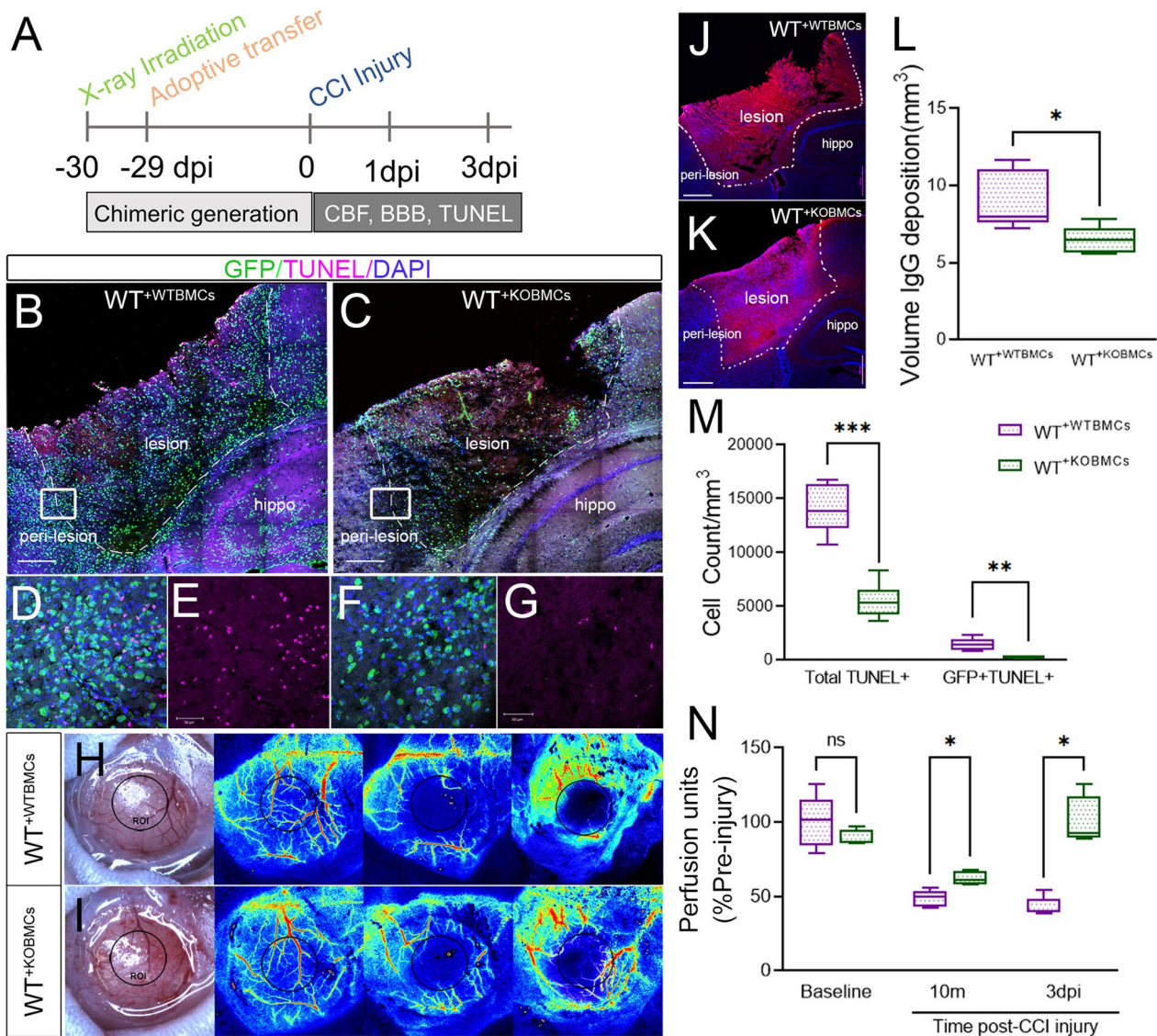


Fig. 7 Peripheral EphA4 deficiency reduces apoptotic cell count and improves cerebral blood flow and BBB stability after CCI injury. **A** Experimental outline. **B–G**, **M** Apoptotic TUNEL+ (purple) cell count is reduced in WT^{+KOBMCs} (**B**, **D**, **E**) compared to WT^{+WTBMCs} (**C**, **F**, **G**) mice. The total number of TUNEL+ and GFP+/TUNEL+ cells (**M**) was counted using image **J** in 3 serial sections using 5 × 7 tiled z-stack confocal images. **H**, **I**, **N** Cerebral blood flow is improved in WT^{+KOBMCs} compared to WT^{+WTBMCs}. Blood flow was measured using laser speckle contrast imaging (LSCI) at 10 min and 3 days post-injury and presented as a percentage perfusion of the baseline. **J–L** Blood–brain barrier permeability is improved in WT^{+KOBMCs} (**K**) compared to WT^{+WTBMCs} (**J**). The volume of IgG deposition was measured at 3 dpi in serial coronal sections using Cavalieri Estimator from StereoInvestigator (**L**). *N* = 5–6 mice/group. Ns = non-significant; **P* < 0.05; ***P* < 0.01; ****P* < 0.001. t-tests (**L**) or multiple t-tests (**M**, **N**). Scale bar = 500 μm in **B**, **C**, **J**, **K** and 50 μm **D–G**

in serial coronal sections at 3 dpi using the optical fractionator probe function on StereoInvestigator (Fig. 7A). The total number of apoptotic cells (total TUNEL+) and apoptotic peripheral-derived immune cells (GFP+TUNEL+) were significantly reduced in WT^{+KOBMCs} compared to WT^{+WTBMCs} mice (Fig. 7B–G, M). This effect was correlated with improved cerebral blood flow and reduced blood–brain barrier

permeability. Cerebral blood flow was measured at 10 min and 3dpi using Laser Speckle Contrast Imaging (LSCI) and calculated as percentage flow from the baseline (pre-injury). WT^{+KOBMCs} showed a significant increase in cerebral blood flow at 3dpi compared to WT^{+WTBMCs} (Fig. 7H, I, N). Blood–brain barrier permeability was measured at 3 dpi by estimating the volume of IgG deposition in serial coronal section using

the Cavalieri Estimator from the Stereoinvestigator software. Significant reduction in IgG deposition was observed in $WT^{+KOBMCs}$ compared to $WT^{+WTBMCs}$, indicating improved blood–brain barrier function and neuroprotection (Fig. 7J–L). We find greater improvements in functional outcome correlate with efferocytosis enhancement by gene deletion of EphA4 on infiltrating innate immune cells.

Discussion

Apoptosis is a prominent mode of cell death that mediates tissue damage and may contribute to the propagation of neuroinflammation following brain injury. In cases of excessive apoptotic cell death, an overwhelmed clearance mechanism may result in the accumulation of apoptotic cells and cellular debris, prolonging the exposure to pro-inflammatory signals and activated immune cells. Therefore, a greater understanding of the efferocytotic process may aid in developing strategies targeting the timely removal of dying cells in the brain. Our results demonstrate an upregulation of “find-me” signal receptors (S1pr1 and Cx3cr1), engulfment receptor (MERTK), and bridging molecules (Gas6 and Pros1) in the damaged cortex, indicating the onset of efferocytosis acutely following trauma. We identified that resident (microglia) and peripheral-derived (monocyte/macrophages; PDMs) myeloid cells show distinct temporal expression patterns of MERTK. Notably, we find that ephrin type-A receptor 4 (EphA4) deficiency on infiltrating immune cells enhanced the capacity of PDMs and peri-lesional microglia for efferocytosis and enhanced cortical expression of *Mertk* and *Gas6* transcripts. Our investigation into the molecular mechanisms revealed increased levels of phosphorylated p-MERTK, p-ERK, and p-Stat6 in the injured cortex of chimeric EphA4 KO mice. In addition, inhibition of ERK and Stat6 attenuated the enhanced efferocytosis and *Mertk* expression in EphA4-deficient BMDMs *in vitro*. This demonstrates that EphA4 suppresses efferocytosis by inhibiting the ERK/Stat6 pathway. These findings highlight a new and novel role for the axon guidance molecule EphA4 in regulating the coordinated process of efferocytosis, which may contribute to the overall neuro-inflammatory milieu after brain injury.

EphA4 has been identified as a regulator of neuroinflammation and secondary injury following brain trauma. Our previous studies utilizing mouse models and bone marrow chimeric approaches have demonstrated that the absence or inhibition of EphA4 in peripheral-derived monocytes/macrophages results in neuroprotection, improved motor function, reduced cortical infiltration of monocytes/macrophages, and a shift in their gene profile from a pro-inflammatory to an anti-inflammatory state [10, 12]. These findings underscore the pivotal role

of EphA4 in mediating the pro-inflammatory phenotypic state of PDM, thereby prompting further investigation into whether EphA4 hampers the adequate clearance of apoptotic debris by modulating the phenotypic state of efferocytes following CCI injury. Interestingly, the deletion of EphA4 on infiltrating immune cells fosters the augmentation of efferocytosis in both PDMs and resident microglia. This may be because EphA4 deficiency in monocytes enhances the expression of *Gas6*, which may fuel the neighboring microglia and promote their efferocytotic abilities. This also suggests that monocytes may have critical properties, allowing them to communicate with and regulate microglial function.

Eph receptors and ephrin ligands facilitate intercellular communication to regulate diverse processes, including adhesion, repulsion, migration, survival, proliferation, remodeling, and differentiation. Upon binding, the clustering of Eph receptors and ligands triggers a cascade of signaling events in both the cells expressing the receptor, and those bearing the ligand [18]. EphA4-null BMDMs, treated with clustered EphA4-FC, showed no effect on efferocytosis efficiency, confirming that forward EphA4 signaling on monocyte/macrophages mediates the suppression of ERK/Stat6 signaling and subsequent enhancement of efferocytosis. Whether the genetic deletion of PDM EphA4 may impair reverse ephrin signaling on apoptotic cells, and its relevance in the current study remains unknown and requires additional investigation. Forward Eph signaling exhibits a remarkable ability to attenuate the RAS-ERK pathway, overriding its activation by other receptor tyrosine kinases [18, 19]. This inhibition has been observed in diverse scenarios, including the modulation of growth cone motility in neurons [20] and the suppression of tumorigenicity in cancer cells [21, 22]. The mechanism underlying Eph receptor-dependent ERK inhibition often involves the activation of the RAS GTPase, p120 RAS GAP, which leads to the subsequent inactivation of H-RAS [23]. Conversely, Eph receptors can activate the RAS-ERK pathway in specific contexts, promoting cellular processes such as proliferation, early gene transcription, cell migration, or repulsion [24, 25]. Eph receptor signaling exerts a complex and context-dependent influence on the RAS-ERK pathway, however, our novel findings indicate that EphA4 suppresses this signaling to limit efferocytosis in the brain following injury.

ERK1/2 signaling modulates multiple aspects of efferocytosis and inflammation resolution, including the regulation of phagocytic receptor expression, cytoskeletal rearrangement, and the production of anti-inflammatory molecules [26, 27]. Activation of the ERK1/2 signaling pathway can enhance the expression of phagocytic receptors, including MERTK, Gas6, MFG-E8, and

integrins (such as $\alpha\beta3$) [28–30]. In addition, ERK1/2 signaling is implicated in promoting actin polymerization and cytoskeletal rearrangement, thereby facilitating the process of efferocytosis [31]. Importantly, ERK1/2 activation also regulates the production of anti-inflammatory mediators during efferocytosis, promoting the polarization of macrophages toward a pro-resolving phenotype, which contributes to sustained efferocytosis and the resolution of inflammation [32, 33]. One crucial transcription factor influenced by ERK1/2 activation to regulate macrophage polarization is Stat6 [34, 35]. The phosphorylation of Stat6 promotes the transcription of genes involved in macrophage pro-resolving and efferocytosis response, such as Gas6 and MERTK [36, 37]. In the present study, we observed an activation of MERTK, ERK1/2, and Stat6 in the injured cortex of chimeric EphA4 KO mice. Furthermore, selective inhibition of ERK and Stat6 reduced efferocytosis and MERTK expression, specifically in EphA4-deficient BMDMS *in vitro*. These findings suggest that EphA4 impedes efferocytosis by inhibiting the P-ERK/P-Stat6/MERTK signaling pathway.

Conclusions

Efferocytosis occurs acutely in the brain following trauma in a limited capacity. Blockade of EphA4 receptor function improves this activity, which coincides with tissue protection and restoration of cerebral blood flow and BBB stability. Unraveling the molecular mechanisms underlying efferocytosis in TBI will lead to new therapeutic avenues promoting this process, mitigating the harmful consequences of apoptotic death, and facilitating optimal recovery following brain trauma.

Abbreviations

AnnV	Annexin V
BM	Bone marrow
BMCs	Bone marrow cells
BMDMS	Bone marrow-derived macrophages
CCI	Controlled cortical impact
Cx3cr1	CX3C motif chemokine receptor 1
EphA	Erythropoietin-producing hepatocellular carcinoma receptors type A
ERK 1/2	Extracellular signal-regulated kinase 1/2
Gas6	Growth arrest-specific 6
GFAP	Glial fibrillary acidic protein
GFP	Green fluorescence protein
IBA1	Ionized calcium-binding adaptor molecule 1
KO	Knock out
LPS	Lipopolysaccharide
LSC	Laser speckle contrast
MERTK	Mer proto-oncogene tyrosine kinase
NeuN	Neuronal nuclei protein
PDMs	Peripheral-derived macrophages
PI	Propidium iodide
ProS1	Protein S
PtdSer	Phosphatidyl serine

S1pr1	Sphingosine-1-phosphate receptor 1
Stat6	Signal transducer and activator of transcription 6
STS	Staurosporine
TBI	Traumatic brain injury
WT	Wild-type
WT ^{+KOBMCs}	EphA4-knockout bone marrow chimeric mice
WT ^{+WTBMCs}	Wild-type bone marrow chimeric mice

Supplementary Information

The online version contains supplementary material available at <https://doi.org/10.1186/s12974-023-02940-5>.

Additional file 1: Figure S1. Low MERTK Expression in astrocytes within the ipsilateral cortex of CCI-injured GFP⁺ bone marrow chimeric wild type (WT^{+WTBMCs}) mice. MERTK (white) is upregulated in GFP⁺ (green, arrowhead) peripheral-derived immune cells and not in the GFAP⁺ (purple) astrocytes in the ipsilateral cortex at 3dpi (A&D-G). The contralateral cortex shows minimal GFAP (purple) expression in astrocytes (arrow) and no detectable MERTK⁺ or GFP⁺ cells (B&H-K). C) The percentage of MERTK-expressing GFP-IBA1⁺ microglia, GFP⁺ IBA1⁺ PDMs, and GFAP⁺ astrocytes was quantified in the ipsilateral cortex at 3dpi using the optical fractionator probe function of StereoInvestigator. *N* = 3–5 mice/group. *****P* < 0.0001. One-way ANOVA followed by Tukey's multiple comparisons test. Scale bar = 50 μ m in A, B and 20 μ m D-K.

Additional file 2: Figure S2. Astrocytes approach and wrap neurons and peripheral immune cells within the ipsilateral cortex of CCI-injured GFP⁺ bone marrow chimeric wild-type (WT^{+WTBMCs}) mice. (A) Representative confocal images for GFAP (purple)- and NeuN (white)-stained coronal section of WT^{+WTBMCs} mice. (B-E) Inset from A, showing GFAP⁺ astrocyte's processes are wrapping GFP⁺ peripheral-derived immune cells (yellow arrowhead) and NeuN⁺ (white) neurons (white arrowhead) in the perilesion cortex at 3dpi. Scale bar = 50 μ m in A and 20 μ m in B-E.

Additional file 3: Figure S3. Chimerism levels in WT^{+WTBMCs} and WT^{+KOBMCs} mice at 1-month after bone marrow transplantation. A-B) Flow cytometry gating strategy to select viable, CD45⁺, GFP⁺, and GFP⁻ leucocytes in the blood of WT^{+WTBMCs} (A) and WT^{+KOBMCs} (B) mice at 1 month following bone marrow transplant. C) Percentage of GFP⁺ and GFP⁻ CD45⁺ leucocytes in WT^{+WTBMCs} and WT^{+KOBMCs} mice.

Additional file 4: Figure S4. Western blot analysis shows the expression of P-MERTK (A), MERTK (B), P-ERK1/2 (B), ERK1/2 (C), and P-Stat6 (D), Stat6 (E), and Actin (F) in the contralateral and ipsilateral cortex of chimeric WT^{+WTBMCs} and WT^{+KOBMCs} mice at 3dpi.

Additional file 5: Figure S5. Induction of apoptosis in Jurkat cells by staurosporine for *in vitro* efferocytosis experiment. Jurkat cells were treated with 1 μ M of Staurosporine (STS) for 3 h and stained with Annexin V (AnnV) and Propidium Iodide (PI). A, C) Representative flow cytometry plots showing the percentage of live (AnnV⁻ PI⁻, Q4), early apoptotic (AnnV⁺ PI⁻, Q3), and late apoptotic (AnnV⁺ PI⁺, Q2) Jurkat cells in the absence (A) or presence (C) of STS treatment. B, D) Representative images taken by ImageStream flow cytometry for live (B) and apoptotic (D) Jurkat cells stained with AnnV (green) and PI (red).

Acknowledgements

We recognize Melissa Markis in the VT College of Veterinary Medicine for support with Flow cytometry.

Author contributions

ES, JL, KGB, IG, JJ, JM, CD, AMK, ME, DP, MC, and XW performed research and analyzed data. ES and MHT wrote and edited the paper, designed the research, and contributed the reagents/analytic tools.

Funding

This work was supported by the National Institute of Neurological Disorders and Stroke of the National Institutes of Health, NS096281, NS119540, and NS121103 (MHT).

Availability of data and materials

Data are available upon request.

Declarations**Ethics approval and consent to participate**

Animal experiments were performed following the NIH Guide for the Care and Use of Laboratory Animals and approved by the Virginia Tech Institutional Animal Care and Use Committee (IACUC; #21-044).

Competing interests

The authors have declared that no conflict of interest exists.

Author details

¹Department of Biomedical Sciences and Pathobiology, Virginia Tech, Blacksburg, VA 24061, USA. ²Department of Pharmacology and Toxicology, Faculty of Pharmacy, Zagazig University, Zagazig, Egypt. ³Translational Biology Medicine and Health Graduate Program, Roanoke, VA 24001, USA. ⁴Center for Engineered Health, Virginia Tech, Blacksburg, VA 24061, USA. ⁵VT-Biomedical Engineering and School of Neuroscience, 970 Washington Street SW, Life Sciences I; Rm 249 (MC0910), Blacksburg, VA 24061, USA.

Received: 18 June 2023 Accepted: 30 October 2023

Published online: 09 November 2023

References

- Miller GF, DePadilla L, Xu L. Costs of nonfatal traumatic brain injury in the United States, 2016. *Med Care*. 2021;59(5):451–5.
- Corrigan F, Mander KA, Leonard AV, Vink R. Neurogenic inflammation after traumatic brain injury and its potentiation of classical inflammation. *J Neuroinflammation*. 2016;13(1):264.
- Russo MV, McGavern DB. Inflammatory neuroprotection following traumatic brain injury. *Science*. 2016;353(6301):783–5.
- Hellewell SC, Morganti-Kossmann MC. Guilty molecules, guilty minds? The conflicting roles of the innate immune response to traumatic brain injury. *Mediators Inflamm*. 2012;2012: 356494.
- Alam A, Thelin EP, Tajsic T, Khan DZ, Khellaf A, Patani R, Helmy A. Cellular infiltration in traumatic brain injury. *J Neuroinflammation*. 2020;17(1):328.
- Akamatsu Y, Hanafy KA. Cell death and recovery in traumatic brain injury. *Neurotherapeutics*. 2020;17(2):446–56.
- Wofford KL, Loane DJ, Cullen DK. Acute drivers of neuroinflammation in traumatic brain injury. *Neural Regen Res*. 2019;14(9):1481–9.
- Das M, Mohapatra S, Mohapatra SS. New perspectives on central and peripheral immune responses to acute traumatic brain injury. *J Neuroinflammation*. 2012;9:236.
- Yang JS, Wei HX, Chen PP, Wu G. Roles of Eph/ephrin bidirectional signaling in central nervous system injury and recovery. *Exp Ther Med*. 2018;15(3):2219–27.
- Kowalski EA, Chen J, Hazy A, Fritsch LE, Gudenschwager-Basso EK, Chen M, Wang X, Qian Y, Zhou M, Byerly M, Pickrell AM, Matson JB, Allen IC, Theus MH. Peripheral loss of EphA4 ameliorates TBI-induced neuroinflammation and tissue damage. *J Neuroinflammation*. 2019;16(1):210.
- Soliman E, Mills J, Ju J, Kaloss AM, Basso EKG, Groot N, Kelly C, Kowalski EA, Elhassany M, Chen M, Wang X, Theus MH. Conditional deletion of EphA4 on Cx3cr1-expressing microglia fails to influence histopathological outcome and blood brain barrier disruption following brain injury. *Front Mol Neurosci*. 2021;14: 747770.
- Kowalski EA, Soliman E, Kelly C, Basso EK, Leonard J, Pridham KJ, Ju J, Cash A, Hazy A, de Jager C, Kaloss AM, Ding H, Hernandez RD, Coleman G, Wang X, Olsen ML, Pickrell AM, Theus MH. Monocyte proinflammatory phenotypic control by ephrin type A receptor 4 mediates neural tissue damage. *JCI Insight*. 2022; 7(15).
- Okyere B, Mills WA 3rd, Wang X, Chen M, Chen J, Hazy A, Qian Y, Matson JB, Theus MH. EphA4/Tie2 crosstalk regulates leptomeningeal collateral remodeling following ischemic stroke. *J Clin Invest*. 2020;130(2):1024–35.
- Okyere B, Giridhar K, Hazy A, Chen M, Keimig D, Bielitz RC, Xie H, He JQ, Huckle WR, Theus MH. Endothelial-specific EphA4 negatively regulates native pial collateral formation and re-perfusion following hindlimb ischemia. *PLoS ONE*. 2016;11(7): e0159930.
- Brickler TR, Hazy A, Guilhaume Correa F, Dai R, Kowalski EJA, Dickerson R, Chen J, Wang X, Morton PD, Whittington A, Ahmed A, Theus MH. Angiotensin/Tie2 axis regulates the age-at-injury cerebrovascular response to traumatic brain injury. *J Neurosci*. 2018;38(45):9618–34.
- Brickler T, Gresham K, Meza A, Coutermarsh-Ott S, Williams TM, Rothschild DE, Allen IC, Theus MH. Nonessential role for the NLRP1 inflammasome complex in a murine model of traumatic brain injury. *Mediators Inflamm*. 2016;2016:6373506.
- Gage MC. Measuring apoptotic cell engulfment (efferocytosis) efficiency. *Methods Mol Biol*. 2019;1951:143–52.
- Lisabeth EM, Falivelli G, Pasquale EB. Eph receptor signaling and ephrins. *Cold Spring Harb Perspect Biol*. 2013;5(9):a009159.
- Darling TK, Lamb TJ. Emerging roles for Eph receptors and ephrin ligands in immunity. *Front Immunol*. 2019;10:1473.
- Meier C, Anastasiadou S, Knoll B. Ephrin-A5 suppresses neurotrophin evoked neuronal motility, ERK activation and gene expression. *PLoS ONE*. 2011;6(10): e26089.
- Macrae M, Neve RM, Rodriguez-Viciano P, Haqq C, Yeh J, Chen C, Gray JW, McCormick F. A conditional feedback loop regulates Ras activity through EphA2. *Cancer Cell*. 2005;8(2):111–8.
- Miao H, Wei BR, Peehl DM, Li Q, Alexandrou T, Schelling JR, Rhim JS, Sedor JR, Burnett E, Wang B. Activation of EphA receptor tyrosine kinase inhibits the Ras/MAPK pathway. *Nat Cell Biol*. 2001;3(5):527–30.
- Minami M, Koyama T, Wakayama Y, Fukuhara S, Mochizuki N. EphrinA/EphA signal facilitates insulin-like growth factor-1-induced myogenic differentiation through suppression of the Ras/extracellular signal-regulated kinase 1/2 cascade in myoblast cell lines. *Mol Biol Cell*. 2011;22(18):3508–19.
- Nakanishi H, Nakamura T, Cavanaugh E, Croce CM. ALL1 fusion proteins induce deregulation of EphA7 and ERK phosphorylation in human acute leukemias. *Proc Natl Acad Sci U S A*. 2007;104(36):14442–7.
- Dail M, Richter M, Godement P, Pasquale EB. Eph receptors inactivate R-Ras through different mechanisms to achieve cell repulsion. *J Cell Sci*. 2006;119(Pt 7):1244–54.
- Luo B, Gan W, Liu Z, Shen Z, Wang J, Shi R, Liu Y, Liu Y, Jiang M, Zhang Z, Wu Y. Erythropoietin signaling in macrophages promotes dying cell clearance and immune tolerance. *Immunity*. 2016;44(2):287–302.
- Jehle AW, Gardai SJ, Li S, Linsel-Nitschke P, Morimoto K, Janssen WJ, Vandivier RW, Wang N, Greenberg S, Dale BM, Qin C, Henson PM, Tall AR. ATP-binding cassette transporter A7 enhances phagocytosis of apoptotic cells and associated ERK signaling in macrophages. *J Cell Biol*. 2006;174(4):547–56.
- Doran AC, Yurdagul A Jr, Tabas I. Efferocytosis in health and disease. *Nat Rev Immunol*. 2020;20(4):254–67.
- Kurihara Y, Nakahara T, Furue M. alphaVbeta3-integrin expression through ERK activation mediates cell attachment and is necessary for production of tumor necrosis factor alpha in monocytic THP-1 cells stimulated by phorbol myristate acetate. *Cell Immunol*. 2011;270(1):25–31.
- Nishi C, Yanagihashi Y, Segawa K, Nagata S. MERTK tyrosine kinase receptor together with TIM4 phosphatidylinositol receptor mediates distinct signal transduction pathways for efferocytosis and cell proliferation. *J Biol Chem*. 2019;294(18):7221–30.
- Lee HG, Minematsu H, Kim KO, Celil Aydemir AB, Shin MJ, Nizami SA, Chung KJ, Hsu AC, Jacobs CR, Lee FY. Actin and ERK1/2-CEBPbeta signaling mediates phagocytosis-induced innate immune response of osteoprogenitor cells. *Biomaterials*. 2011;32(35):9197–206.
- Kumar D, Pandit R, Yurdagul A Jr. Mechanisms of continual efferocytosis by macrophages and its role in mitigating atherosclerosis. *Immunometabolism (Cobham)*. 2023;5(1): e00017.
- Pastore M, Caligiuri A, Raggi C, Navari N, Piombanti B, Di Maira G, Rovida E, Piccinni MP, Lombardelli L, Logiodice F, Rombouts K, Petta S, Marra F. Macrophage MerTK promotes profibrogenic cross-talk with hepatic stellate cells via soluble mediators. *JHEP Rep*. 2022;4(4): 100444.
- Tripathi P, Sahoo N, Ullah U, Kallionpaa H, Suneja A, Lahesmaa R, Rao KV. A novel mechanism for ERK-dependent regulation of IL4

transcription during human Th2-cell differentiation. *Immunol Cell Biol.* 2012;90(7):676–87.

35. Takeda K, Tanaka T, Shi W, Matsumoto M, Minami M, Kashiwamura S, Nakanishi K, Yoshida N, Kishimoto T, Akira S. Essential role of Stat6 in IL-4 signalling. *Nature.* 1996;380(6575):627–30.
36. Brunn A, Mihelcic M, Carstov M, Hummel L, Geier F, Schmidt A, Saupe L, Utermohlen O, Deckert M. IL-10, IL-4, and STAT6 promote an M2 milieu required for termination of P0(106–125)-induced murine experimental autoimmune neuritis. *Am J Pathol.* 2014;184(10):2627–40.
37. Cai W, Dai X, Chen J, Zhao J, Xu M, Zhang L, Yang B, Zhang W, Rocha M, Nakao T, Kofler J, Shi Y, Stetler RA, Hu X, Chen J. STAT6/Arg1 promotes microglia/macrophage efferocytosis and inflammation resolution in stroke mice. *JCI Insight.* 2019; 4(20).

Publisher's Note

Springer Nature remains neutral with regard to jurisdictional claims in published maps and institutional affiliations.

Ready to submit your research? Choose BMC and benefit from:

- fast, convenient online submission
- thorough peer review by experienced researchers in your field
- rapid publication on acceptance
- support for research data, including large and complex data types
- gold Open Access which fosters wider collaboration and increased citations
- maximum visibility for your research: over 100M website views per year

At BMC, research is always in progress.

Learn more biomedcentral.com/submissions

